



Fast Fourier ptychographic quantitative phase microscopy for in vitro label-free imaging: supplement

RUOFEI WU,¹  ZICONG LUO,¹  MINGDI LIU,¹ HAIQI ZHANG,¹ JUNRUI ZHEN,¹ LISONG YAN,² JIAXIONG LUO,¹ AND YANXIONG WU^{1,3,*}

¹*School of Physics and Optoelectronic Engineering, Foshan University, Foshan 528000, China*

²*School of Optical and Electronic Information, Huazhong University of Science and Technology, Wuhan 430074, China*

³*Ji Hua Laboratory, Foshan, Guangdong 528200, China*

*wuyanxiong@fosu.edu.cn

This supplement published with Optica Publishing Group on 6 December 2023 by The Authors under the terms of the [Creative Commons Attribution 4.0 License](https://creativecommons.org/licenses/by/4.0/) in the format provided by the authors and unedited. Further distribution of this work must maintain attribution to the author(s) and the published article's title, journal citation, and DOI.

Supplement DOI: <https://doi.org/10.6084/m9.figshare.24624783>

Parent Article DOI: <https://doi.org/10.1364/BOE.505267>

FAST FOURIER PTYCHOGRAPHIC QUANTITATIVE PHASE MICROSCOPY FOR IN VITRO LABEL-FREE IMAGING: SUPPLEMENTAL DOCUMENT

1. Analysis of LR images obtained via the FQP-FPM method in pure-phase sample experiments

In this section, we extend the simulation experiment presented in Section 3.1 of the main text, with all parameter settings kept the same, including the input pure-phase sample GT (USAF), as shown in Fig. 3(a). The LR images acquired by the FQP-FPM method are shown in Fig. S1. The section above the dashed line shows the spectral coverage of each subaperture of the BF setup (the blue color represents the portion of the spectrum containing the BF low-frequency information) as well as the LR images acquired in the corresponding airspace. As the subaperture center position is set at $NA_{ill} = NA_{obj}$, the LR images acquired with asymmetric sequential illumination are rich in low-frequency phase-contrast information, which is similar to the four phase-contrast images (top, bottom, left, and right) acquired with the biaxial DPC method, and they can complete the spectral filling in the range of $2NA_{obj}$ and realize the recovery of the low-frequency phase information. The section below the dashed line shows the full DF image acquisition, where we set up 12 LEDs on the annulus with $NA_{ill} = 2NA_{obj}$, and the LR image acquired at this position does not contain any low-frequency information about the BF transmissive light, but exclusively contain high-frequency information about the samples from the scattered light. Each symmetric subaperture pair, as represented by the red frame in Fig. S1, is the DF image acquired by the parallel acquisition strategy based on symmetric illumination, while next to it are the two DF images captured by asymmetric sequential illumination (indicated by the blue frame). As our input GT is a pure-phase sample, the high-frequency phase-lining information (qualitative characterization of phase information) of the sample can be seen from the sequentially acquired images, which is the most commonly used acquisition strategy for FPM, and quantitative phase recovery can be achieved from these acquired LR images by the phase recovery algorithm. Meanwhile, the image captured by parallel acquisition based on symmetric illumination can be regarded as a summation of each sequentially acquired image (superposition of high-frequency phase-lining information), which is consistent with that defined by Eq. (6). Afterwards, the images are demultiplexed and quantitative phase recovery is achieved by a modified phase recovery algorithm (as described in Section 2.3).

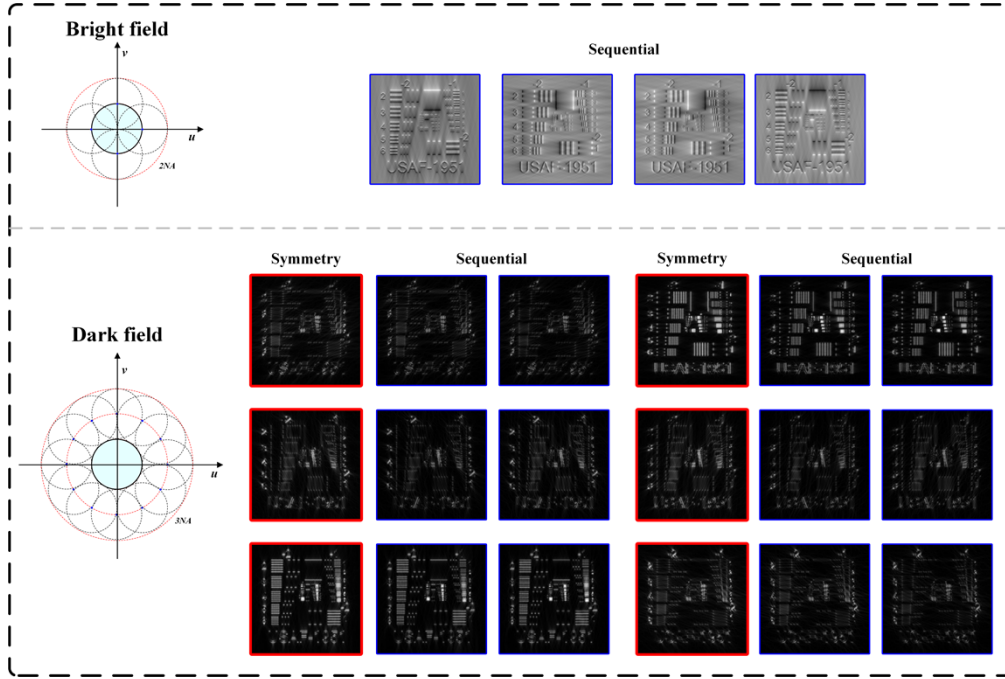


Fig. S1. Simulation of bright- and dark-field images acquired using the proposed FQP-FPM method on pure-phase samples (USAF).

2. Simulation of real experimental reconstruction of the FQP-FPM method in the presence of noise

In this section we discuss the reconstruction effect of the proposed FQP-FPM method with other methods in noisy real experimental situations.

The basis remains the analog simulation experiments in Section 3.1 of the manuscript, and all the experimental parameter settings remain the same. On this basis, we added 10% random noise to all the acquired LR images. As before, we compared the reconstruction results of the three methods (conventional FPM, QP-FPM, and FQP-FPM methods), as shown in Fig. S2(b1)–(d3). It is easy to see that all three methods result in the degradation of imaging quality owing to the effect of noise. Combined with Table S1, the conventional FPM method decreases less because the larger data redundancy provides more tolerance for errors, and the SSIM index decreases from the original 0.9610 to 0.8942; The QP-FPM method, which has been downsampled but not used a parallel acquisition strategy, does not have such a high fault tolerance, and the SSIM index decreases from the original 0.9571 to 0.8985, and some uneven distribution of the background can be observed, while the phase contrast appears to be degraded; The imaging quality degradation of the FQP-FPM with symmetric parallel acquisition is more pronounced (the SSIM index decreases from the original 0.9567 to 0.7753), which is in agreement with the observation, mainly due to the fact that the demultiplexing strategy is more susceptible to the experimental noise (which affects the spectral distribution of the acquired images, and thus interferes with the subsequent decoherence and iterative process).

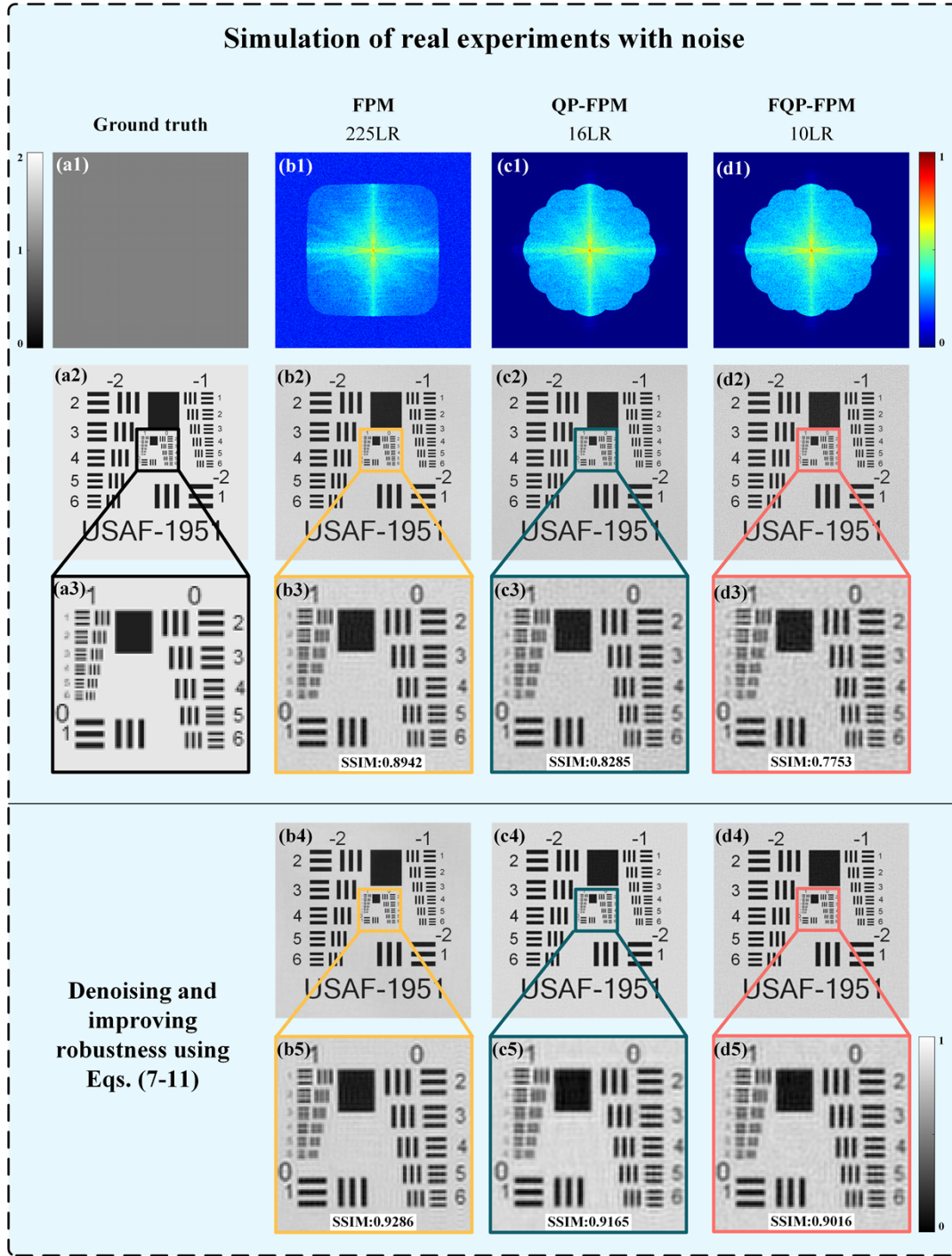


Fig. S2. FQP-FPM Validation via pure-phase sample (USAF) reconstruction in simulation experiments (adding 10% random noise and denoising). (a) Ground-truth amplitude and phase images of complex transmittance function used to simulate sample. (b1)–(d3) Spectrum and phase reconstructed using the conventional FPM, QP-FPM, and FQP-FPM methods in the noisy case (without denoising) with their ROI amplification regions. (b4)–(d5) Reconstructed phases and their ROI-amplified regions in the noisy case (using Eqs. 7–11 to improve robustness to noise) for the conventional FPM, QP-FPM, and FQP-FPM methods.

Therefore, in the original manuscript, Eqs. (7) – (11) introduce the reconstruction algorithm of FQP-FPM, which first uses an improved thresholding method [50] for noise reduction of the image and then optimizes the spectral updating strategy (based on the improvement of the ePIE), which further improves the robustness of the algorithm to noise and achieves fast convergence [28,46]. As shown in Fig. S2(b4)–(d5), the reconstruction quality is improved after the operation of the above methods (SSIM is above 0.9), among which the improvement of the parallel acquisition method (FQP-FPM) is the largest, which fully illustrates the importance of the relevant steps in Section 2.3.

Table S1. Evaluation of reconstruction effectiveness (using SSIM index) comparing three methods (conventional FPM, QP-FPM and FQP-FPM) for reconstruction without noise, addnoise, and after improving robustness to noise

	FPM	QP-FPM	FQP-FPM
	SSIM		
Noise-free (From table 1 of the manuscript)	0.9610	0.9571	0.9567
Addnoise (10% random noise)	0.8942	0.8285	0.7753
Improving robustness to noise (Using manuscript Eqs. 7–11)	0.9286	0.9165	0.9016

3. Exploring the data redundancy requirements of the FQP-FPM method

The FQP-FPM method was designed to quickly obtain subaperture information on the target NA. However, the reconstruction quality must be simultaneously guaranteed to make the most "cost-effective" choice. After the introduction of the acquisition strategy and simulation experiments of the FQP-FPM method in Sections 2.2 and 3.1, we determined the reconstruction of the low-frequency phase information using four LR images at the location of $NA_{\text{ill}} = NA_{\text{obj}}$. The subaperture located at $NA_{\text{ill}} = 2NA_{\text{obj}}$ can provide a better supplement for missing low-frequency information. Based on this, we discuss the number of subapertures and their data redundancy for the dark-field high-frequency information setup, as shown in Fig. S3. Fig. S3(a) shows the subaperture filling model for the dark-field high-frequency information. To generalize the conclusions of this study, we adopted the intensity and phase shown in Fig. S4(a) as GT. We set up 8–16 subapertures in the dark field and used the proposed FQP-FPM method to realize quantitative phase reconstruction of complex-amplitude samples, and used the structural similarity error (1-SSIM) to assess the quality of the reconstructed phase. The variation curve with the number of dark-field subaperture settings is shown in Fig. S3(b). From the curves, we can easily observe that the number of subapertures is set to 12, which is the "watershed" of the curve slope. When the number of subapertures is less than 12, the quality of the phase reconstruction increases sharply with an increase in the number of subapertures (the decline in the error curve is steeper). When the number of subapertures is greater than 12, the improvement in the reconstructed phase quality as the number of subapertures increases is more limited (the error curve hardly declines). Therefore, setting the number of dark-field subapertures to 12 was the most "cost-effective" solution. The calculated spectral overlap rate was 40.75% (considering only the neighboring subapertures whose centers were located at NA_{ill}

$= 2NA_{obj}$). This concept can be generalized to the study of data redundancy for higher synthetic apertures (NA_{syn}).

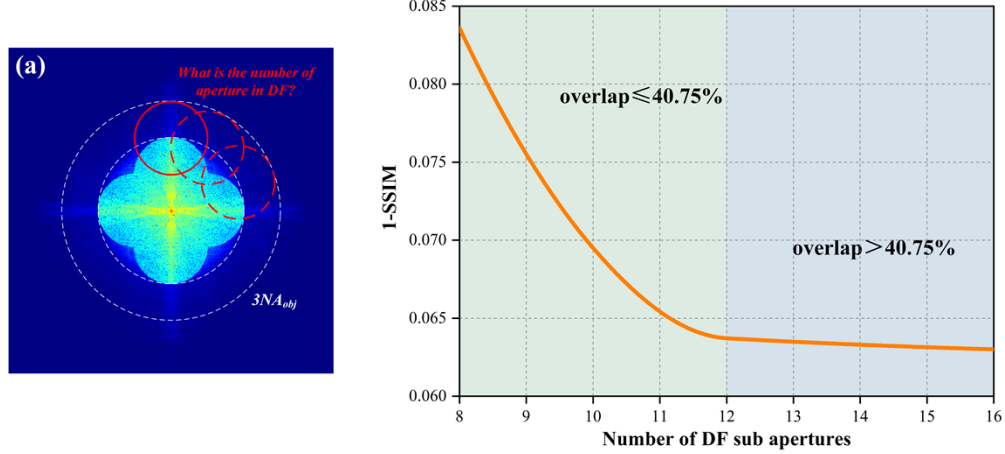


Fig. S3. Data redundancy exploration of the FQP-FPM method. (a) Simulated dark-field subaperture spectral filling model. (b) Probing the effect of the number of subaperture fills at the dark-field location on the quality of the FQP-FPM reconstruction.

4. Validation of complex-amplitude sample reconstruction using the FQP-FPM method

In this paper, the FQP-FPM method is presented in terms of FPM with phase reconstruction; however, this does not mean that it can only be imaged on pure-phase samples. For general samples (with both intensity and phase information), FQP-FPM can also demonstrate its intensity reconstruction performance. As shown in Fig. S4(a), we input both the intensity and phase information as GT. The experimental parameters for the remaining simulations were the same as those presented in Section 3.1. Figs. S4(b)–(d) show the intensity and phase images reconstructed using the FPM, QP-FPM, and FQP-FPM methods, respectively. The SSIMs with GT were calculated and are shown below the images to evaluate the reconstruction quality. The SSIMs of the reconstructed intensity for the QP-FPM and FQP-FPM methods, compared to the conventional FPM method, exhibit differences of 0.0285 and 0.0291, respectively. Despite this difference, they can reconstruct the intensity information. The phase reconstruction is similar to that presented in Section 3.1; both the QP-FPM after annular downsampling and the FQP-FPM after further using a symmetric illumination-based parallel acquisition strategy at the DF are able to better reconstruct the phase (with small differences of 0.0014 and 0.0016 from the SSIM of the conventional FPM, respectively). The difference between the intensity and phase reconstruction performance of the FQP-FPM method is mainly due to the different absorption and phase transfer functions of the samples in the low-frequency region [38], as well as a certain degree of influence after downsampling. Therefore, we can conclude that under dark-field parallel acquisition or sequential acquisition, the image contains the phase-contrast information of the sample, and the image of the dark-field parallel acquisition is equivalent to the superposition of the information of the sequential acquisition image. Decoherence and phase reconstruction can be realized via subsequent algorithm improvements.

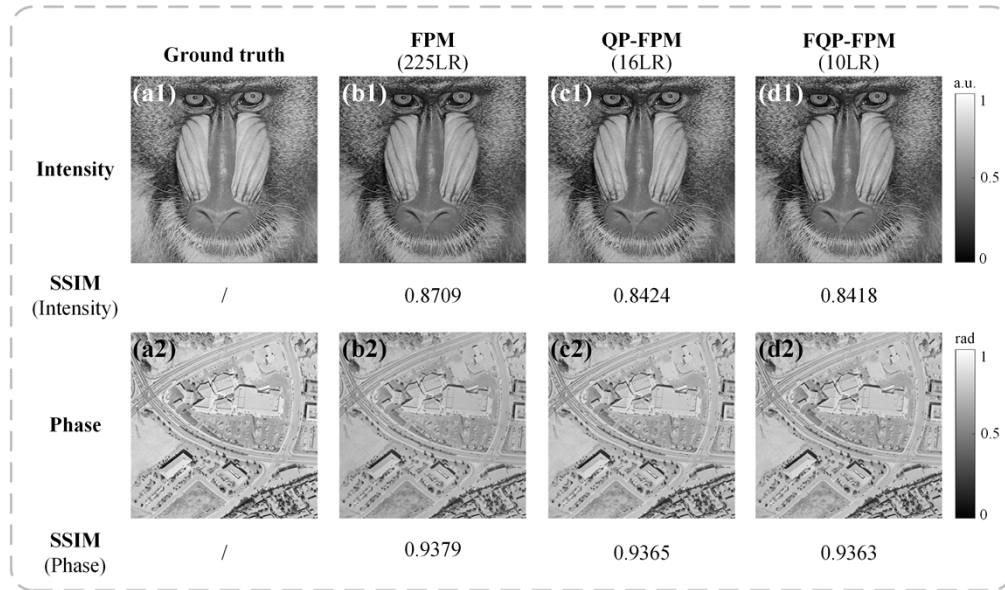


Fig. S4. Validation of the FQP-FPM imaging using conventional analog simulations (simulating samples with both intensity and phase). All other parameter settings remain the same as those described in Section 3.1. (a) Input ground-truth intensity and phase images. (b) Intensity and phase images reconstructed using the conventional FPM method. (c) Intensity and phase images reconstructed using the QP-FPM method. (d) Intensity and phase images reconstructed using the FQP-FPM method.